Rett Syndrome Mutation MeCP2 T158A Disrupts DNA Binding, Protein Stability and ERP Responses

Darren Goffin[1], **Megan Allen**[1,5], **Le Zhang**[1,5], **Maria Amorim**[1,5], **I-Ting Judy Wang**[1,5], **Arith-Ruth S. Reyes**[1], **Amy Mercado-Berton**[2], **Caroline Ong**[4], **Sonia Cohen**[4], **Linda Hu**[4], **Julie A. Blendy**[2], **Gregory C. Carlson**[3], **Steve J. Siegel**[3], **Michael E. Greenberg**[4], and **Zhaolan (Joe) Zhou**[1,*]

[1]Department of Genetics, University of Pennsylvania School of Medicine, Philadelphia, PA 19104

[2]Department of Pharmacology, University of Pennsylvania School of Medicine, Philadelphia, PA 19104

[3]Department of Psychiatry, University of Pennsylvania School of Medicine, Philadelphia, PA 19104

[4]Department of Neurobiology, Harvard Medical School, Boston, MA 02115

Abstract

Mutations in the *MECP2* gene cause the autism spectrum disorder Rett Syndrome (RTT). One of the most common mutations associated with RTT occurs at MeCP2 Threonine 158 converting it to Methionine (T158M) or Alanine (T158A). To understand the role of T158 mutation in the pathogenesis of RTT, we generated knockin mice recapitulating MeCP2 T158A mutation. Here we show a causal role for T158A mutation in the development of RTT-like phenotypes including developmental regression, motor dysfunction, and learning and memory deficits. These phenotypes resemble those in *Mecp2*-null mice and manifest through a reduction in MeCP2 binding to methylated DNA and a decrease in MeCP2 protein stability. Importantly, the age-dependent development of event-related neuronal responses are disrupted by MeCP2 mutation, suggesting that impaired neuronal circuitry underlies the pathogenesis of RTT and that assessment of event-related potentials may serve as a biomarker for RTT and treatment evaluation.

*Correspondence: Zhaolan@mail.med.upenn.edu.
[5]These authors contributed equally to this work.

INTRODUCTION

RTT is an autism spectrum disorder caused by mutations in the X-linked gene encoding methyl-CpG binding protein 2 (MeCP2)[1]. RTT is associated with different types of mutations within *MECP2*, including missense, nonsense, deletions and insertions[2]. Classical RTT patients, irrespective of the type of mutation, develop normally for the first 6–18 months of age, after which they enter a period of regression characterized by deceleration of head growth and a loss of acquired motor and language skills. Frequently, patients develop stereotypic hand wringing, abnormal breathing, seizures and autistic behaviors[3]. The molecular mechanisms through which different types of *MECP2* mutations lead to disruptions in proper brain function are not fully understood.

Mice engineered with different *Mecp2* alterations present phenotypes that are both similar and distinct from those observed in *Mecp2*-null mice[4–11]. These similarities and differences in mouse models suggest that different *MECP2* mutations are likely to have both shared and distinct biochemical and physiological correlates. Intriguingly, reintroduction of MeCP2 into behaviorally affected *Mecp2*-null mice is sufficient to rescue RTT-like phenotypes[12] and restoration of MeCP2 function in astrocytes alone significantly improve the developmental outcome of *Mecp2*-null mice[13], suggesting that RTT is reversible upon restoration of MeCP2 function. Thus, understanding the mechanisms by which different MeCP2 mutations lead to RTT may reveal effective strategies tailored to the particular mutation to restore MeCP2 function.

Mutation of the Threonine 158 (T158) residue, located at the C-terminus of the methyl-CpG binding domain (MBD) of MeCP2, represents one of the most common mutations observed in RTT. Approximately 10% of all RTT cases carry a single nucleotide mutation converting T158 to Methionine (T158M) or in rare cases to Alanine (T158A)[2]. The T158 residue has been suggested to play an important structural role in the stabilization of the MBD and the binding of MeCP2 to methylated DNA[14]. Whether mutation of T158 leads to MeCP2 gain-of-function or loss-of-function, however, is not clear.

The onset of RTT symptoms occurs during the establishment and refinement of neural networks in early postnatal development. Studies in *Mecp2*-null mice have suggested that reductions in connectivity between excitatory pyramidal neurons are associated with RTT-like phenotypes[15–17]. How reductions in neuronal connectivity lead to the manifestation of the age-dependent cognitive and behavioral deficits in RTT is currently unknown. Cognitive dysfunctions are frequently assessed by measuring the neurophysiological responses that occur during passive processes or during the performance of cognitive, sensory or motor tasks. Brain activations that occur during these tasks manifest as event-related potentials (ERPs). Disruptions in ERPs and the oscillations that underlie them are associated with a number of cognitive disorders such as schizophrenia[18,19] and autism[20,21]. EEG recordings in *Mecp2*-null mice[22,23] and ERP recordings in RTT patients[24,25] also suggest that alterations in brain activity are associated with behavioral and cognitive deficits. How ERPs are affected by MeCP2 dysfunction and how changes in EEG and ERPs correlate with the age-dependent progression of RTT-like symptoms, however, remains to be determined.

Given the high frequency of T158 mutations in RTT and its role in methyl-DNA binding, we sought to model this mutation *in vivo* and developed knockin mice containing MeCP2 T158A mutation. We found that these mice recapitulate a number of RTT-like symptoms observed in *Mecp2*-null mice including late onset of hypoactivity, poor motor control, irregular breathing, altered anxiety, impaired learning and memory, and shortened lifespan. We demonstrated that T158A mutation decreases the binding of MeCP2 to methylated DNA *in vitro* and *in vivo,* and reduces MeCP2 protein stability. Moreover, the amplitude and latency of ERPs in both MeCP2 T158A and *Mecp2*-null mice are significantly altered. Time-frequency analysis of these ERPs revealed that MeCP2 T158A mice failed to show a developmental increase in event-related power and phase locking in contrast to wild-type (WT) mice, demonstrating that MeCP2 is required for the development of functional neuronal circuits. Our studies suggest that stabilization of MeCP2 protein and enhancement of its affinity for methylated DNA may provide a potential therapeutic approach to treat patients with MeCP2 T158 mutation. Furthermore, assessment of ERPs may serve as a biomarker for RTT and the evaluation of therapeutic efficacy in RTT treatment.

RESULTS

Generation of MeCP2 T158A and loxP knockin mice

Although mutation of MeCP2 T158A occurs at a lower frequency than T158M in RTT patients, the mechanism through which both mutations impair MeCP2 function is believed to be the same: the lack of hydroxyl group in alanine and methionine destabilizes the tandem Asx-ST motif in the MBD and thus reduces MeCP2 affinity for methylated DNA[14]. Indeed, patients carrying MeCP2 T158A or T158M mutation are phenotypically similar in the identity and severity of presented symptoms[26,27]. To examine the importance of the T158 residue in the functioning of MeCP2, we developed a knockin mouse with T158A mutation to circumvent the potential steric interference brought about by the larger Methionine residue. To facilitate screening of properly targeted ES cells, we incorporated a silent mutation at codon 160 to create a new BstEII restriction site and a floxed Neomycin expression cassette in intron III of the *Mecp2* gene (Supplementary Fig. 1). Given that our goal was to test a rather subtle mutation on MeCP2 – a single amino acid change of T158A – we also engineered loxP knockin mice that contain the BstEII restriction site and loxP insertion but that lack T158A mutation, to rule out the possibility that manipulation of the *Mecp2* locus may affect MeCP2 expression (Supplementary Fig. 1). Sequencing of MeCP2 mRNA extracted from brain tissues of WT, *Mecp2*$^{T158A/y}$, and *Mecp2*$^{loxP/y}$ mice verified that both *Mecp2*$^{T158A/y}$ and *Mecp2*$^{loxP/y}$ knockin mice contained the T to C mutation at codon 160 for the generation of the BstEII restriction site, whereas only *Mecp2*$^{T158A/y}$ mice contain the A to G mutation at codon 158 (Fig. 1a). Furthermore, an MeCP2 T158 site-specific antibody, recognized MeCP2 protein from WT and *Mecp2*$^{loxP/y}$ mice, but not *Mecp2*$^{T158A/y}$ mice confirming the successful generation of MeCP2 T158A knockin mice (Fig. 1b).

MeCP2 T158A mice recapitulate RTT-like phenotypes

RTT is characterized by relatively normal development during the first 6–18 months of life, followed by a period of developmental stagnation leading to motor impairments, breathing

abnormalities, and intellectual disability. We evaluated the presence, development and progression of RTT-like phenotypes in MeCP2 T158A mice following a previously reported scoring system[12]. We found that male $Mecp2^{T158A/y}$ mice present no overt symptoms during the first 4 weeks of life, but become progressively symptomatic after 5 weeks of age as indicated by significantly increasing phenotypic score (Fig. 1c). The hindlimb clasping apparent in $Mecp2$-null mice is also observed in $Mecp2^{T158A/y}$ mice (Supplementary Fig. 2a). $Mecp2^{T158A/y}$ mice weighed significantly less than their WT littermates starting from 4 weeks of age but then gradually gained weight to WT levels after 8 weeks (Supplementary Fig. 2b). In contrast, the body weights of $Mecp2^{loxP/y}$ mice are indistinguishable from their WT littermates (data not shown). Occasionally, we also observed seizure behaviors in $Mecp2^{T158A/y}$ mice after 5 weeks of age.

Given that $MECP2$ is an X-linked gene and that the majority of RTT patients are girls with mosaic MeCP2 expression due to random X-chromosome inactivation, female $Mecp2^{T158A/+}$ mice represent a close genetic match to RTT patients. Phenotypic scoring revealed no apparent symptoms in these mice until 17 weeks of age, after which they become progressively and increasingly symptomatic (Fig. 1d). A significant increase in body weight also occurred in female $Mecp2^{T158A/+}$ mice at the time of symptom presentation (Supplementary Fig. 2c) similar to that observed in heterozygous $Mecp2^{-/+}$ female mice[12].

An early diagnostic criterion for RTT is a deceleration in head growth often leading to microcephaly by the first two years of life[3,28]. We observed a significant reduction in the sizes and weights of brains of presymptomatic (P30) and postsymptomatic (P90) $Mecp2^{T158A/y}$ mice relative to their WT littermates (Fig. 1e), similar to that observed in $Mecp2$-null mice[4,5]. The gross brain anatomy of $Mecp2^{T158A/y}$ mice, however, was indistinguishable from their WT littermates (Supplementary Fig. 2d). The decreased brain size and weight in $Mecp2$-null mice are purported to occur, at least in part, through a reduction in neuronal soma size[4,28]. To assess whether soma size is affected in $Mecp2^{T158A/y}$ mice, we bred MeCP2 T158A mice to those expressing GFP under the control of the $Thy1$ promoter[29]. Focusing on the hippocampal CA1 region, confocal imaging of GFP-positive pyramidal neurons revealed a significant reduction in soma size in $Mecp2^{T158A/y}$ mice compared to WT littermates at both P30 and P90 (Fig. 1f).

MeCP2 mutation in boys often leads to infantile lethality[3] and male $Mecp2$-null mice show shortened life span[4,5,8]. We find that male $Mecp2^{T158A/y}$ mice die prematurely, with 50% dying by 16 weeks of age (Fig. 1g), which is approximately 3–4 weeks longer that germline $Mecp2$-null mice[4,5]. No apparent changes in the survival profiles of female $Mecp2^{T158A/+}$ mice were observed before 6 months of age (data not shown). Importantly, we have not observed any significant difference in longevity, body weights or brain weights of $Mecp2^{loxP/y}$ knockin mice, supporting the conclusion that these changes are the result of T158A mutation (data not shown). Together, these data demonstrate that mice carrying MeCP2 T158A mutation manifest RTT-like phenotypes.

MeCP2 T158A mice present similar phenotypes to *Mecp2*-null mice

Given the clinical relevance of MeCP2 T158A mutation, we sought to carry out a side-by-side comparison of behavioral phenotypes with a well-studied *Mecp2*-null mouse [5]. In light of the locomotor deficits, aberrant gait and hindlimb clasping observed in these mice (Supplementary Video 1), we assessed locomotor activity in a home cage environment with a cohort of age-matched WT, $Mecp2^{T158A/y}$ and $Mecp2^{-/y}$ littermates on the same C57BL/6 background at approximately 9 weeks of age. We found a significant reduction in the locomotor activity of both $Mecp2^{T158A/y}$ and $Mecp2^{-/y}$ mice compared to WT littermates (Fig. 2a). However, the reduction in locomotor activity was significant higher in $Mecp2^{-/y}$ mice compared to $Mecp2^{T158A/y}$ mice (Fig. 2a). We also found a significant reduction in distance traveled by $Mecp2^{T158A/y}$ mice at 11 but not 3 weeks compared to WT littermates using the open field assay (Supplementary Fig. 3a). Similarly, locomotor activity is also significantly reduced in female $Mecp2^{T158A/+}$ mice at 20 weeks, but not 12 weeks of age (Supplementary Fig. 3b), consistent with the age-dependent hypoactivity observed with phenotypic scoring (Fig. 1c,d).

To examine motor coordination and motor learning in these two mouse models, we performed the accelerating rotarod test. WT mice show an increase in the latency to fall over the course of 4 trials per day and over 4 consecutive days, indicating improvements in motor coordination and learning over time (Fig. 2b). However, both $Mecp2^{T158A/y}$ and $Mecp2^{-/y}$ mice spent significantly less time on the rotarod compared to WT littermates and failed to improve significantly over the course of 4 days suggestive of deficits in motor coordination and motor learning (Fig. 2b). The latency to fall from the rotarod was moderately but significantly decreased in $Mecp2^{-/y}$ mice compared $Mecp2^{T158A/y}$ mice (Fig. 2b). We conclude that MeCP2 T158A mutation impairs motor function similar to that seen in RTT patients and to a lesser degree than *Mecp2*-null mice.

RTT patients experience anxiety episodes, particularly in response to distressing events[3]. The role of MeCP2 in anxiety in mice, however, is less clear: *Mecp2*-null mice and mice with a 50% reduction in MeCP2 protein expression both show a decreased anxiety phenotype[8], whereas those containing an early-truncating mutation show increased anxiety[6]. Using the elevated zero maze paradigm, we found that $Mecp2^{T158A/y}$ and $Mecp2^{-/y}$ mice spend significantly less time in the closed arm and significantly more time in the open arm compared to their WT littermates (Fig. 2c). This suggests that T158A mice show reduced anxiety similar to those observations in *Mecp2*-null mice and mice with decreased MeCP2 protein expression.

Because RTT is the primary cause of intellectual disability in females, we examined whether MeCP2 mutant mice have learning and memory deficits using contextual and cued fear conditioning paradigms. Mice were trained to associate a context (testing box) and a cue (auditory tone) with a coterminating foot shock. Animals typically freeze in response to the shock. We found no differences in freezing behaviors in WT and $Mecp2^{T158A/y}$ littermates prior to or immediately following shocks, suggesting no differences in pain sensitivity. However, $Mecp2^{-/y}$ mice exhibit significantly increased freezing even prior to the shock (Supplementary Fig. 3c). This is likely due to their decreased locomotor activity and

akinesia, thus confounding interpretation of the fear-conditioning test. These mice were therefore excluded from this study. 24 hours after training, $Mecp2^{T158A/y}$ mice demonstrate significantly less context- and cue-dependent freezing compared to their WT littermates, suggesting deficits in learning and memory (Fig. 2d).

Together, these data demonstrate that MeCP2 T158A knockin mice present phenotypes similar to those observed in $Mecp2$-null mice but to a lesser extent overall. We therefore infer that T158A is a partial loss-of-function mutation.

Decreased MeCP2 protein stability in MeCP2 T158A mice

Alterations in MeCP2 protein levels, such as a 50% reduction or a two-fold increase, leads to the progressive development of neurological deficits in mice, albeit at much later time points than those observed in $Mecp2$-null mice[7,9,10]. We therefore examined whether T158A mutation alters the expression of MeCP2 protein during development. Quantitative Western blotting on whole-cell lysates from the brains of male $Mecp2^{T158A/y}$ mice revealed that MeCP2 protein expression is significantly decreased at P2, P30 and P90 compared to their WT littermates (Fig. 3a). The down-regulation of MeCP2 expression is significantly higher at P90, when $Mecp2^{T158A/y}$ mice present overt RTT-like phenotypes, than at either P2 or P30, when symptoms are not present (Fig. 1c). Importantly, MeCP2 protein levels were not affected in $Mecp2^{loxP/y}$ mice indicating that the down-regulation of MeCP2 is due to the presence of the T158A mutation rather than genomic modification (Fig. 1b). These changes in MeCP2 expression are likely to be independent of gene transcription since quantitative RT-PCR found no significant differences in the level of MeCP2 mRNA expression between $Mecp2^{T158A/y}$ and WT mice at P0, P30 or P90 (Supplementary Fig. 4). Despite RTT being primarily a neurological disorder[3], MeCP2 is ubiquitously expressed in all mammalian tissues[30]. Indeed, we found that MeCP2 protein levels are decreased to a similar extent in kidney, liver, lung and heart in $Mecp2^{T158A/y}$ mice (Fig. 3b).

MeCP2 protein levels are also significantly decreased in the brains of female $Mecp2^{T158A/+}$ mice compared to their WT littermates (Fig. 3c). The magnitude of MeCP2 down-regulation in females is less than that observed in male $Mecp2^{T158A/y}$ mice and is likely due to the mosaic expression of MeCP2 T158A in heterozygous $Mecp2^{T158A/+}$ mice. To investigate whether mutation at T158 disrupts MeCP2 protein expression in human RTT patients, we obtained fibroblast cultures derived from a female RTT patient with T158M mutation and an age-matched female control. We found that MeCP2 expression is also significantly down-regulated by about 40% in cells with MeCP2 T158M mutation compared to control cells (Fig. 3c). These data demonstrate that T158 mutation, to either A or M, triggers the down-regulation of MeCP2 protein expression in both humans and mice, indicating that the reduction in MeCP2 protein expression may be a contributing factor to RTT.

To investigate whether the reductions in MeCP2 protein levels are the consequence of decreased protein stability, we cultured embryonic day 16 cortical neurons isolated from WT and $Mecp2^{T158A/y}$ mice and inhibited new protein translation using Cycloheximide (CHX). The stability of existing MeCP2 protein was assessed at 0, 3, 6 and 9 hours following CHX treatment. We found that MeCP2 protein levels in WT neurons remain relatively constant over the course of the 9-hour CHX treatment compared to vehicle-treated cultures (Fig. 3d).

In contrast, MeCP2 T158A protein levels are significantly reduced following 6-and 9-hour CHX treatments (Fig. 3d), suggesting that T158A mutation decreases MeCP2 protein levels by increasing its rate of degradation. We did not observe destabilization of other proteins such as NeuN in T158A mice (Fig. 3d). Therefore, the development of MeCP2 T158A knockin mice has uncovered a novel function of T158 in the stabilization of MeCP2 protein *in vivo*. The reduction in MeCP2 protein stability mediated by T158A mutation may contribute, at least in part, to the etiology of RTT.

T158A mutation disrupts MeCP2 binding to methylated DNA

Located at the 3′-end of the MBD, T158 is believed to play an important role in stabilizing the tertiary structure of MBD and is critical for the binding of MeCP2 to methylated DNA[14]. We recapitulated these *in vitro* observations using a Southwestern assay (Fig. 4a). To examine the role of T158 in the regulation of MeCP2 binding to methylated DNA *in vivo*, we isolated nuclei from brains of WT and *Mecp2^{T158A/y}* mice and performed chromatin immunoprecipitation (ChIP) assays against several known MeCP2 binding loci. MeCP2 has been previously shown to bind across a 39 kb promoter region of the *Bdnf* locus tracking methyl-CpG sites[31]. Consistent with this, we found a similar MeCP2 binding pattern in brains from P60 WT mice (Fig. 4b). MeCP2 ChIP over the same region in *Mecp2^{T158A/y}* brains, however, revealed a 70–75% reduction in MeCP2 binding across the entire locus (Fig. 4b), suggesting that T158A mutation decreases MeCP2 binding at methylated DNA. To validate this finding, we also analyzed the binding of MeCP2 to the *Xist*, *Snrpn* and *Crh* loci, known MeCP2 binding targets[31,32] and found that the binding of MeCP2 at these loci is significantly reduced by approximately 70% in *Mecp2^{T158A/y}* brains (Fig. 4c). Thus, the reduction in MeCP2 binding at the *Bdnf*, *Xist*, *Snrpn*, and *Crh* loci likely reflects a decreased binding of MeCP2 T158A to methylated DNA together with reduced MeCP2 protein expression.

We reasoned that if MeCP2 T158A has a reduced affinity to methylated DNA *in vivo*, WT or MeCP2 T158A protein would be extracted differently from nuclei under the same salt conditions. To biochemically assay the reduced affinity of MeCP2 T158A to methylated DNA, we isolated neuronal nuclei from either WT or *Mecp2^{T158A/y}* mouse brains and treated them with increasing concentrations of NaCl to extract proteins into the supernatant. Quantitative Western blot analysis revealed that MeCP2 T158A protein is extracted more readily than WT protein under low salt conditions of 250mM and 300mM NaCl (Fig. 4d). When the salt is raised to above 350 mM, both WT and T158A protein are extracted to a similar degree. Thus, mutation of T158A appears to decrease the affinity of MeCP2 for DNA.

MeCP2 predominantly associates with heterochromatic foci in mouse cell nuclei in an MBD- and DNA methylation-dependent manner, resulting in a characteristic punctate pattern of nuclear staining[33]. Indeed, we demonstrated that MeCP2 immunoreactivity is observed throughout the nucleus with particularly high enrichment at heterochromatin-dense foci in nuclei from P90 WT neurons (Fig. 4e). In contrast, in nuclei from P90 *Mecp2^{T158A/y}* neurons, MeCP2 is markedly diffuse with a clear absence of co-localization with DNA, indicating that the binding of MeCP2 to methylated DNA is disrupted (Fig. 4e). This

difference is unlikely due to changes in heterochromatin formation as no overt differences are seen in DNA staining in T158A mice. We observed similar immunoreactivity patterns in P30 $Mecp2^{T158A/y}$ mice prior to symptom presentation (data not shown). Furthermore, MeCP2 immunoreactivity in female $Mecp2^{T158A/+}$ mice shows a mosaic expression of MeCP2 with approximately 50% of nuclei showing MeCP2 immunoreactivity at heterochromatin-dense foci with the remaining exhibiting diffuse immunoreactivity (Fig. 4f), as is expected due to random X-chromosome inactivation. Notably, the intensity of MeCP2 immunoreactivity is decreased in T158A neurons compared to WT neurons, consistent with a reduction of MeCP2 T158A protein expression. Together, these data demonstrate that T158A mutation impairs the binding of MeCP2 to methylated DNA *in vivo* and contributes, at least in part, to the etiology of RTT.

Disruption of MeCP2 binding to methylated DNA

Transcriptional profiling of RNA isolated from the hypothalamus or cerebellum of *Mecp2*-null mice revealed changes in the expression of thousands of genes, with many of these changes in a tissue-specific manner[32]. We analyzed the expression of a few representative targets such as *Bdnf*, *Crh* and *Sgk* using quantitative RT-PCR and found that both *Bdnf* and *Crh* transcription are significantly reduced in the hypothalamus but not striatum of T158A mice (Fig. 5a,b), whereas, *Sgk*, a gene that is upregulated in *Mecp2*-null mice[34], is elevated in the striatum but not in the hypothalamus of T158A mice (Fig. 5a,b). These data support that gene transcription is similarly disrupted in MeCP2 T158A and *Mecp2*-null mice in a tissue- and/or cell-type specific manner.

MeCP2 has been shown to regulate gene transcription through its interaction with histone deacetylases (HDACs) 1 and 2 and the co-repressor Sin3a[35,36]. It is conceivable that T158A mutation may disrupt the ability of MeCP2 to associate with these proteins through alterations in the conformation of MeCP2 and thus disrupt downstream gene regulation. We therefore performed co-immunoprecipitation experiments using an antibody against MeCP2 in nuclear extracts prepared from WT and $Mecp2^{T158A/y}$ brains. Consistent with previous studies, WT MeCP2 interacts with HDAC1 and Sin3a (Fig. 5c). We also detected the association of MeCP2 T158A with HDAC1 and Sin3A, albeit at a reduced level consistent with the reduced MeCP2 T158A protein expression (Fig. 5c). Thus, these data support that MeCP2 T158A protein retains the ability to interact with the co-repressor proteins. Together, we conclude that MeCP2 T158A leads to a deregulation of gene expression through reduced DNA binding and MeCP2 protein stability.

Age-dependent alterations in EEG and ERP recordings

The manifestation of symptoms in RTT patients and *Mecp2*-null mice are thought to occur in part due to alterations in neural network activity. Since RTT symptoms appear at certain developmental time points, we sought to investigate the neural mechanisms underlying age-dependent exhibition of phenotypes in MeCP2 T158A mice. Thus, we performed EEG recordings in WT and $Mecp2^{T158A/y}$ mice at two developmental time periods, P30 and P90; that is, prior to and subsequent to the establishment of RTT-like symptoms. EEG recordings in awake, freely mobile mice demonstrated a significant increase in the power of high-gamma frequency (γ_{high}; 70–140 Hz) oscillations in $Mecp2^{T158A/y}$ mice at P90 compared to

WT littermates (Fig. 6a,b). A similar increase in γ_{high} power was also observed in symptomatic $Mecp2^{-/y}$ mice (Supplementary Fig. 5a,b). γ_{high} activity is known to be associated with epilepsy in the EEG before and during the seizure[37] and may thus reflect an overall hyperexcitability in the brains of $Mecp2^{T158A/y}$ and $Mecp2^{-/y}$ mice[22]. However, we did not observe a significant increase in γ_{high} power in pre-symptomatic $Mecp2^{T158A/y}$ mice at P30 (Supplementary Fig. 6a,b), suggesting that MeCP2 dysfunction induces hyperexcitability in the brain in an age-dependent manner.

In addition to measuring electrical activity during passive processes, it is also possible to measure those that occur during the performance of a cognitive, sensory or motor task. The manifestation of these brain activities is recorded as a series of amplitude deflections in the EEG as a function of time and is referred to as an event-related potential (ERP). ERPs are small compared to the background EEG but can be resolved by averaging single trial epochs. They are characterized as voltage deflections defined by latency and polarity where the amplitude and latency of the polarity peaks are believed to reflect the strength and timing of the cognitive processes related to the event. Notably, RTT patients, as well as patients with schizophrenia and autism, are reported to show alterations in both the amplitudes and latencies of ERP[19–21,24,25].

To examine ERP responses in $Mecp2^{T158A/y}$ mice, we performed EEG recordings following the presentation of a series of white noise clicks. We chose to perform auditory-evoked ERP assessments since they can be performed on freely mobile mice and are not confounded by the motor or attentional deficits associated with MeCP2 dysfunction. The ERP was extracted by averaging the EEG traces over single trial epochs. ERPs in WT and $Mecp2^{T158A/y}$ mice show a stereotypical initial positive peak (P1), followed by a negative peak (N1) and a subsequent second positive peak (P2) (Fig. 6c). Interestingly, we found significant increases in the latency and significant reductions in the amplitudes of the N1 and P2 peaks in symptomatic P90 $Mecp2^{T158A/y}$ mice compared to WT littermates (Fig. 6c–e). Similar alterations in ERP amplitudes and latencies were observed in $Mecp2^{-/y}$ mice (Supplementary Fig 5c–e). However, we observed no significant effect on ERPs in $Mecp2^{T158A/y}$ mice at P30, prior to the establishment of RTT-like symptoms (Supplementary Fig 6c–e). Importantly, we found no differences in hearing sensitivities between $Mecp2^{T158A/y}$ mice or $Mecp2^{-/y}$ mice and their WT littermates as measured by auditory brain stem responses, suggesting that these disruptions in ERP are due to alterations in cortical processing of sensory input (Supplementary Fig. 7). These data suggest that neural networks underlying information processing are disrupted by MeCP2 dysfunction in an age-dependent manner, corresponding to the behavioral onset of symptoms.

Progressive alterations in event-related power and PLF

One limitation of time-amplitude analysis of ERPs is that oscillatory information not time-locked to the stimulus is lost through signal averaging. Using time-frequency analysis it is possible to analyze changes in oscillatory activity as a function of time and thus gain additional insight into the underlying brain activity and circuitry. Oscillatory responses during the performance of tasks are characterized by the average power and phase locking across trials[38]. The degree of event-related power and phase locking at different frequencies

may reflect the strength and connectivity of local (at high frequencies) and long-range (at low frequencies) neuronal circuits[39].

Thus, we next performed time-frequency analysis on EEG recordings used to determine auditory-evoked ERPs. We found that the presentation of an auditory stimulus modulated the mean event-related power in a frequency-specific manner. WT mice at P90 showed a significant depression in the mean power of oscillations in the low-frequency delta (δ; 2–4 Hz), theta (θ; 4–8 Hz) and alpha (α; 8–12 Hz) ranges upon auditory stimulation (Fig. 7a,b). The mean event-related power of high-frequency beta (β; 12–30 Hz), low gamma (γ_{low}; 30–50 Hz) and high gamma (γ_{high}; 70–140 Hz) increased following the auditory stimulus and was followed by a sustained depression in power (Fig. 7a,b). Notably, these changes are sustained for a number of oscillation cycles at all frequencies and outlast the transient ERP response reflecting an effect in both evoked and ongoing oscillatory processes (Fig. 7a,b). Overlaying the ERP with band-pass EEG traces at each frequency range reveals the oscillatory information within the transient ERP response (Supplementary Fig. 8). $Mecp2^{T158A/y}$ mice, however, exhibited significantly attenuated event-related power in both low- and high-frequency oscillations at P90 when RTT-like symptoms are overt (Fig. 7a,b and Supplementary Fig. 9a). Similarly, highly symptomatic $Mecp2^{-/y}$ mice show significantly reduced event-related power following auditory stimulation at all frequencies (Supplementary Fig. 9b, 10a,b). Notably, we also found a significant reduction in event-related power in low-frequency δ, θ and α in P30 $Mecp2^{T158A/y}$ mice prior to symptom onset compared to WT littermates (Supplementary Fig. 9c, 11a,b). These data suggests that the underlying deficits in neural activity occur prior to the establishment of behavioral symptoms consistent with *in vitro* electrophysiological studies showing reduced cortical excitability in $Mecp2^{-/y}$ mice even at 2–3 weeks of age[15].

Time-frequency analysis also allows for the calculation of oscillation phase locking across trials. The phase locking factor (PLF) quantifies the trial-to-trial reliability of oscillation phase with a high PLF corresponding to a low circular variance in oscillation phase as a function of time between trials. High PLF is thought to reflect the reliability and sensitivity of communications between circuits in the brain[40]. We find that WT mice at P90 show significant increases in PLF at all frequencies in response to the presentation of auditory stimuli (Fig. 7c,d). The increase in PLF in $Mecp2^{T158A/y}$ mice at P90, however, is significantly reduced compared to WT mice (Fig. 7c,d and Supplementary Fig. 9d). A significant reduction in event-related PLF in $Mecp2^{-/y}$ mice was also observed, consistent with the expression of RTT-like phenotypes in both groups of mice (Supplementary Fig. 9e, 10c,d). We also detected significant attenuation in PLF in pre-symptomatic P30 $Mecp2^{T158A/y}$ mice, although only at δ-and high-gamma frequencies (Supplementary Fig. 9f, 11c,d). Importantly, the fact that we do not observe changes in ERP amplitudes at P30 in $Mecp2^{T158A/y}$ mice (Supplementary Fig. 6, 12) suggests that time-frequency analysis of event-related power and PLF represents a sensitive approach to probe neural function *in vivo*.

Interestingly, when comparing the event-related neuronal responses in WT mice at two developmental stages, we find that event-related power at all frequencies and PLF at high frequencies are significantly higher in P90 mice than those at P30 (Fig. 8a,b). This likely

reflects the development and maturation of the underlying neuronal circuitry. In contrast, *Mecp2*$^{T158A/y}$ mice do not show a developmental increase in either event-related power (Fig. 8c) or phase locking (Fig. 8d) from P30 to P90, suggesting an impairment in age-dependent neural network maturation. These age-dependent differences are only observed using time-frequency but not time-amplitude analysis (Fig. 8 and Supplementary Fig. 12). Together, these data reveal that MeCP2 plays an important role in the regulation of event-related neuronal responses and is required for the maturation and restructuring of neural networks. The disruptions in event-related power and PLF may therefore contribute to the deficits in behavioral and cognitive functions observed in RTT. We propose that ERP studies may serve as a sensitive biomarker for the evaluation of treatments in RTT patients.

DISCUSSION

Mutation of MeCP2 T158 to M or in rare cases to A represents one of the most common mutations observed in RTT patients[2]. Previous *in vitro* experiments established a critical role for this residue in the binding of MeCP2 to methylated DNA. To address the causal role of T158A mutation in the pathogenesis of RTT and the role of methyl-DNA binding in the proper functions of MeCP2, we developed and characterized MeCP2 T158A knockin mice. We found that MeCP2 T158A mice develop normally for the first 4–5 weeks of life after which they present RTT-like symptoms including decreased motor performance, altered anxiety, aberrant gait, hindlimb clasping, breathing abnormalities, and impaired learning and memory. The similarity in the identity and severity of symptoms with those observed in *Mecp2*-null mice indicates that MeCP2 T158A mutation is a partial loss-of-function mutation.

The development of this mouse line allowed us to investigate the biochemical consequences of MeCP2 T158A mutation *in vivo*. In agreement with previous *in vitro* studies, we find that MeCP2 T158A mutation leads to a reduction in the affinity of MeCP2 for methylated DNA *in vivo*. Surprisingly, we also observed that T158A mutation concomitantly decreases MeCP2 protein expression *in vivo*. Consistent with these data, we find that fibroblasts obtained from a female RTT patient carrying MeCP2 T158M mutation express decreased levels of MeCP2 protein. These findings reveal two consequences of T158 mutation: impaired MeCP2 binding to DNA and decreased MeCP2 protein stability of MeCP2.

Previous studies have demonstrated that MeCP2 protein levels must be tightly regulated to ensure its proper function. A 50% reduction in MeCP2 protein levels leads to progressive neurological symptoms[9,10], although symptoms appeared later and do not fully recapitulate RTT-like symptoms as in *Mecp2*-null mice. Therefore, the destabilization of MeCP2 protein alone, as observed in our T158A mice, may not be sufficient to cause the RTT-like symptoms. We propose that the combined reduction in MeCP2 protein levels and the decreased binding to methylated DNA contribute to the loss-of-function phenotype in T158A knockin mice. The development of knockin mice carrying other mutations that disrupt DNA binding will provide further insights into this hypothesis. Given that the reintroduction of MeCP2 protein into *Mecp2*-null mice is sufficient to rescue RTT-like phenotypes[12] we suggest a dual approach to restore MeCP2 function in patients carrying MeCP2 T158 mutations: increasing MeCP2 affinity for methylated DNA and enhancing

MeCP2 protein stability. Indeed, the feasibility of increasing affinity for DNA has been shown for other DNA-binding proteins such as p53[41]. It is conceivable that increasing MeCP2 affinity to methylated DNA may help stabilize MeCP2 protein expression. Targeting one or both of these possibilities may lead to the amelioration of RTT-like phenotypes. Our study also suggests that different therapeutic strategies should be considered for treating patients with different MeCP2 mutations.

Given their neurological origin, many of the symptoms associated with RTT have been hypothesized to result from imbalanced neural networks[3]. Evidence to support this arises from observed alterations in synaptic connectivity and plasticity[12,15–17,42] and hyperexcitability in the EEG[22,23] of *Mecp2*-null mice. Furthermore, ERP analysis in RTT females suggests alterations in sensory processing of information[24,25]. Given the delayed onset of symptoms in RTT patients, MeCP2 T158A mice and *Mecp2*-null mice, we sought to examine whether neurophysiological responses as measured by EEG were altered during development in MeCP2 T158A mice. Indeed, we found that the power of high-gamma EEG signals is significantly increased in MeCP2 T158A mice when these mice exhibit RTT-like symptoms, suggesting hyperexcitability in the brain. Furthermore, assessment of auditory-evoked ERPs revealed a significant and marked reduction in the amplitude and increased latency of ERPs in MeCP2 T158A and *Mecp2*-null mice suggesting deficits in information processing in the brain similar to that observed in RTT females[24,25], autism[20,21] and other disorders including schizophrenia[18]. Further studies are needed to address the neuronal mechanisms that underlie these deficits in ERP response.

Our data show that disturbances in event-related power and phase locking also occur in MeCP2 mouse models and may play a role in the etiology of RTT. In humans and animal models, changes in the power and phase locking of neuronal responses coordinate neuronal activity across different brain regions. These changes are involved in the development and efficacy of motor, perceptual and memory tasks and deficits in neuronal oscillations are consistently observed in neurological disorders in which these functions are impaired[18,43]. Our findings that both low- and high-frequency event-related oscillations are disrupted lead us to hypothesize that deficits in local and long-distance neuronal circuitry occur following MeCP2 dysfunction. The neurophysiological mechanisms that lead to disturbances in these oscillations are not known, but may involve the reduced neuronal connectivity that leads to a redistribution of neuronal activity away from excitation and towards inhibition as observed in *Mecp2*-null mice[15–17]. Furthermore, given the important role that event-related neuronal responses play in the development of the nervous system[44], their disruption prior to symptom presentation may augment the deficits in neuronal activity caused by MeCP2 dysfunction. Indeed, MeCP2 T158A mice do not exhibit developmental increases in event-related power or phase locking suggestive of stagnation in the developmental of neuronal circuits. Moreover, our findings that event-related changes in power and phase locking occur in MeCP2 T158A mice with no behavioural symptoms suggest that disruptions in neuronal networks may precede the behavioral RTT-like phenotypes. The identification of the mechanisms that lead to these disturbances will provide valuable insights into the pathogenesis of RTT and the neuronal networks underlying manifestation of behavioral phenotypes in RTT.

In summary, the development of MeCP2 T158A mice has uncovered a novel role for T158 in the pathogenesis of RTT and revealed an alternative strategy to restore MeCP2 function. These mice provide an *in vivo* animal model for assessing therapeutic efficacy in pre-clinical trials. Moreover, given that ERP studies can be readily performed in humans, assessment of ERP and the changes in oscillation and phase locking may serve as a valuable biomarker for evaluating RTT phenotypes.

METHODS

Generation of MeCP2 T158A and loxP knockin mice

The targeting construct used for homologous recombination in ES cells was cloned in two arms by PCR amplification of sv129 genomic DNA. The 5′ arm was PCR amplified with primers 5′-AGGAGGTAGGTGGCATCCTT-3′ and 5′-CGTTTGATCACCATGACCTG-3′while the 3′ arm was PCR amplified with 5′-GAAATGGCTTCCCAAAAAGG-3′ and 5′-AAAACGGCACCCAAAGTG-3′ primers. Novel restriction sites at the ends of each arm were created using nested primers for cloning into a vector containing a floxed Neomycin cassette (Neo) and a diphtheria toxin-A negative-selection cassette. MeCP2 Threonine 158 was mutated to Alanine using QuickChange (Stratagene) site-directed mutagenesis. A single nucleotide at codon T160 also underwent site-directed mutagenesis for a silent mutation to introduce a novel BstEII restriction site in order to identify correctly targeted ES cells.

The targeting construct was confirmed by sequencing, linearized using NotI and subsequently electroporated into sv129 mouse ES cells. Two MeCP2 T158A ES cell clones and two loxP ES cell clones were independently injected into C57BL/6 blastocysts and subsequently implanted into pseudopregnant females. The resulting chimeric offspring were mated with C57BL/6 *EIIa-Cre* mice for embryonic deletion of the Neo cassette, and the agouti offspring were screened by PCR genotyping to confirm germ line transmission of the T158A allele or loxP allele.

Animal husbandry

Experiments were conducted in accordance with the ethical guidelines of the National Institutes of Health and with the approval of the Institutional Animal Care and Use Committee of the University of Pennsylvania. All experiments described were performed using animals on a congenic sv129:C57BL/6 background with the mutation backcrossed to C57BL/6 mice (Charles River) for at least five generations, unless otherwise stated. Mice were genotyped using a PCR-based strategy to detect the residual loxP sequence remaining in intron III after Cre-mediated excision of the Neomycin cassette. The genotyping primers (5′-GGATTGTGGAAAAGCCAG-3′ and 5′-ATGACCTGGGCAGATGTGGTAG-3′) give rise to a 620bp product from the WT *Mecp2* allele and 691bp for the *Mecp2 T158A* allele.

Neuronal cell culture

Cortical cultures were prepared from embryonic day 16 (E16) mouse embryos similar to that previously described[45]. For analysis of protein stability, cultures were treated with vehicle

(DMSO) or 100 μM Cycloheximide (Sigma) for 3, 6 or 9 hours before lysis in 1X SDS sample buffer.

Quantitative Western analysis

Quantitative Western blot was performed using Odyssey Infrared Imaging System (Licor). Antibodies used include a rabbit polyclonal antibody directed against the C-terminal of MeCP2 (1:1,000)[46], mouse anti-NeuN (1:500; Chemicon), and rabbit anti-histone H3 (1:10,000; Upstate). Secondary antibodies used were anti-rabbit IRDye 680LT and anti-mouse IRDye 800CW (Licor). Quantification of protein expression levels was carried out following Odyssey Infrared Imaging System protocols.

Quantitative RT-PCR

For measurements of gene expression in brain tissues, total RNA was isolated using Trizol reagent (Invitrogen) and treated with TURBO DNase (Ambion). 1 μg of total RNA was reverse-transcribed by oligodT-priming using SuperScriptIII reverse transcriptase (Invitrogen). Quantitative real-time PCR was performed on 10 ng of the resulting cDNA using SYBR Green detection (Applied Biosystems). All qPCR primer pairs are exon-spanning and are available upon request. All mRNA levels of genes of interest were normalized to β-tubulinIII mRNA levels.

Immunohistochemistry

Mice were anesthetized with 1.25% Avertin, transcardially perfused with 4% paraformaldehyde, postfixed overnight at 4°C. Immunohistochemistry was performed on 20 μm free-floating sections as previously described[47]. Tissues were incubated with primary antibodies in blocking solution (rabbit anti-total MeCP2; 1:1,000) overnight at 4°C. Fluorescence detection was performed using anti-rabbit Alexa Fluor-488 conjugated secondary antibody (2.67 μg/ml; Invitrogen) for 1 hour at room temperature (RT). Sections were counterstained with TOPRO-3 (1:1,000; Invitrogen) to visualize DNA. Images were acquired using a Leica confocal microscope. Images were acquired using identical settings for laser power, detector gain amplifier offset and pinhole diameter in each channel.

Chromatin Immunoprecipitation (ChIP)

Mouse forebrain tissues were homogenized in cross-linking buffer (1% formaldehyde, 100 mM HEPES pH7.5, 100 mM NaCl, 1mM EDTA, 1 mM EGTA) and cross-linked for 10 minutes at RT. After quenching with 125 mM glycine, cross-linked tissue was washed with ice-cold PBS and dounced 12 strokes in lysis buffer (50 mM HEPES pH 7.5, 140 mM NaCl, 1mM EDTA, 1 mM EGTA, 10% Glycerol, 0.5% NP-40, 0.25% Triton X-100 with protease inhibitors). Nuclei were pelleted, washed, and resuspended in chromatin buffer (10 mM Tris-HCl pH 8.0, 1 mM EDTA, 0.5 mM EGTA with protease inhibitors). Sonication was performed to break chromatin into sizes from 400 bp to 2 kb. Salt and detergent were added to adjust the chromatin buffer to 0.5% Triton X-100, 150 mM NaCl, 10 mM EDTA, and 10% DOC. For immunoprecipitation, rabbit polyclonal antisera directed against total MeCP2 (5 μl) was coupled to 10 μl Protein A Dynabeads (Invitrogen) in the absence or presence of 1 μg of the peptide from which antisera was raised (for a peptide blocking

control). Chromatin immunoprecipitation was performed at 4°C overnight. Precipitated chromatins were washed 6 times with wash buffer (10 mM Tris pH8.0, 320 mM LiCl, 10 mM EDTA, 0.5% Triton, 0.1% DOC with protease inhibitors). Chromatins were eluted twice with elution buffer (50 mM Tris-HCl pH 8.0, 10 mM EDTA, 1% SDS), digested with proteinase K (0.5 mg/ml) and reverse-crosslinked at 65°C overnight. After RNAse A treatment, DNA fragments were extracted with phenol/chloroform, precipitated with ethanol, and purified with a Qiaquick PCR purification column. The amount of DNA fragments of interest in ChIPs was measured by quantitative real-time PCR using SYBR green detection. All qPCR primer sequences are available upon request.

EEG surgery

Animals underwent stereotaxic implantation of tripolar electrode assemblies (PlasticsOne) for non-anesthetized recording of auditory ERPs. Animals were anesthetized with isoflurane (4% for induction; 1.5–2% for surgery with 1 liter/min O_2). Three stainless steel electrodes, mounted in a single pedestal were aligned to the sagittal axis of the skull. A stainless steel recording electrode was placed 2.0 mm posterior, 2.0 mm left lateral relative to bregma and 1.8 mm depth (Supplementary Fig. 13). Ground and reference electrodes were placed anterior of the hippocampal electrode at 1.0 mm and 2.0 mm distances respectively. The electrode pedestal was secured to the skull with ethyl cyanoacrylate and dental cement. Post-operative analgesia was supplied using the opioid analgesic, buprenorphine (buprenex, s.c., 0.1 μg/g body weight). Mice were allowed to recover for 7 days prior to EEG recordings.

EEG Recordings

EEG recordings were performed on freely mobile, non-anesthetized mice in their home cage environment after 20-minute acclimation to the recording room. Recordings were performed using Spike2 software connected to a Power 1401 II interface module (CED) and high impedance differential AC amplifier (A-M Systems). Signals were acquired at 1,667 Hz and band pass filtered between 1 and 500 Hz with a 60 Hz notch filter and gain of 1,000.

ERPs were recorded by presentation of auditory stimuli consisting of a series of 250 white-noise clicks of 10 ms duration, 85-dB sound pressure and 4-second interstimulus interval. Stimuli were presented through speakers on the recording chamber ceiling (Model 19–318A, 700–10,000 Hz frequency response, Radioshack) connected to a digital audio amplifier (RCA Model STAV3870, Radioshack). ERP traces were generated by averaging across single trial epochs centered at $t = 0 \pm 2$ seconds. Single trials were baseline corrected by subtracting the temporal mean at $t = -1$ s to $t = 0.5$ s. Altering the baseline closer to sound presentation had no effect on the results shown. The mean ERP amplitudes were subsequently calculated across 250 trials.

Time-frequency analysis of EEG

For each recording where mice were presented with 250 white-noise clicks (10 ms duration, 85-dB sound pressure, 4-second interstimulus interval) we computed event-related power and phase as a function of frequency and time. Event-related power changes and phase-locking were determined similar to that described previously[38,48]. EEG signal was filtered into bands with center frequencies ranging from 2 – 140 Hz in 1 Hz steps and 2 Hz

bandwidths. The raw signal was filtered using a two-way least squares FIR filter. The Hilbert transform was applied to create a complex-valued time series, *V(t)*:

$$V(t)=v(t)+iu(t)$$

where the real part, *v(t)* is the same as the normalized filtered EEG and the imaginary part *u(t)* is from the Hilbert transform of *v(t)*, given by:

$$u(t)=\frac{1}{\pi}PV\int_{-\infty}^{+\infty}\frac{V(t')}{(t-t')}dt'$$

and PV signifies the Cauchy Principal Value. Analytic power, *P(f,t)*, as a function of frequency *f* and time *t* is given by:

$$P(f,t)=v(f,t)^2+u(f,t)^2$$

We determined changes in event-related power by isolating single trial epochs of 4-second duration with *t = 0* representing sound presentation ± 2 seconds. We determined power response relative to the prestimulus basis for each trial. We used a baseline of the mean power at t = −1 s to t = 0.5 s. Altering the baseline period did not affect the conclusions of the study. The mean power across the 250 trials was subsequently calculated.

The instantaneous phase time series $\theta(f,t)$ was determined as function of time and frequency by taking the two-argument four quadrant arctangent (atan2) of the real parts of *v(t)* and *u(t)* such that phase values were in the range from −π to π.

$$\theta(f,t)=2\arctan\frac{u(f,t)}{\sqrt{v(f,t)^2+u(f,t)^2}+v(f,t)}$$

An example of EEG amplitudes and phase calculated using this method for 1-second epoch of EEG recorded in a P90 WT mouse is shown (Supplementary Fig. 14). Event-related phase locking was measured using a PLF by calculating 1 circular variance of instantaneous phase measurements, defined as:

$$PLF=1-\frac{1}{n}\sqrt{\sum_{k=1}^{n}(\cos\theta_k)^2+\sum_{k=1}^{n}(\sin\theta_k)^2}$$

Basal EEG power measurement

Basal EEG power was determined across a 60 second period during a period of wakefulness as assessed by behavioral monitoring of mice. For each 60-second recording, we computed the power as a function of frequency and time with frequency varying between 2 and 140 Hz using 1 Hz increments. To measure the power at frequency *f*, we filtered the data between *f*

± 1 Hz, then calculated power using the Hilbert transform as described above. The power for each 60-second recording was calculated as the mean power across individual 1-second epochs during this 60-second period. The relative power at each individual frequency was presented as a fraction of the sum of powers at all frequencies. These relative powers were then separated into frequency bins and calculated as the area under the curve. Relative power measurements for MeCP2 T158A or *Mecp2*-null were then expressed as a percentage of WT.

ABR Recordings

Auditory brainstem responses (ABR) recordings were performed using the same equipment and electrode placement as other recordings except EEG signals were acquired at 15,625 Hz. Auditory stimulation consisted of 4,000 white-noise clicks of 3 ms duration with 125 ms interstimulus interval at seven sound pressures: decreasing from 85- to 55-dB. EEG signal was digitally filtered between 100 and 500 Hz and EEG amplitudes averaged across trials centered at $t = 0$ seconds representing sound presentation. The average ABR consists of 5 amplitude peaks and the amplitudes of these peaks decrease with decreasing sound pressure[49].

Behavioral Assays

All behavioral studies were carried out blinded to genotype where possible. Due to the presence of overt RTT-like symptoms in MeCP2 T158A mice and *Mecp2*-null mice, the identity of the genotype was sometimes noticeable but care was taken to avoid bias. For all studies, the mice were allowed to habituate to the testing room for 30 minutes prior to the test and testing was performed at the same time of day.

Phenotypic scoring—Phenotypic scoring was performed on a weekly basis for the absence or presence of RTT-like symptoms as described previously[12].

Locomotor assay—Locomotor activity was measured by beam-breaks in a photobeam frame (Med Associates, St. Albans, VT, USA). Mice were placed into a clean home cage-like environment lined with bedding and resting within a photobeam frame. The number of beam breaks as a measure of locomotor activity was quantified over 5 minutes.

Accelerating rotarod—Mice at approximately 9 weeks were placed on an accelerating rotarod apparatus (Med Associates, St Albans, VT, USA) for 16 trials (four trials a day on four consecutive days) with at least 15-minute rest interval between trials. Each trial lasted for a maximum of 5 minutes, during which the rod accelerated linearly from 3.5 to 35 rpm. The amount of time and rpm for each mouse to fall from the rod was recorded for each trial.

Elevated Zero Maze—The elevated zero maze was performed by placing mice in one of the closed quadrants and their movement traced over the course of 5 minutes. Analysis was performed with TopScan software (Clever Systems).

Fear conditioning—Mice were placed in individual chambers (Med Associates, St. Albans, VT, USA) for 2 minutes followed by a loud tone (85 dB, 2kHz) for 20 seconds, co-

terminating with a 2-second 0.75 mA foot-shock. Mice were left undisturbed for one minute, after which a second pairing of sound cue and shock was delivered. 90 seconds after the second shock, mice were returned to their home cage. Freezing behavior, defined as no movement except respiration, was determined pre- and post- tone-shock pairings and scored by FreezeScan NI version 2.00. To test for context-dependent learning, mice were placed back into the same testing boxes 24 hours later without a tone or shock for 5 minutes. One hour later, animals were placed into a novel chamber and tested for cued fear memory. Two minutes after entering this chamber, the "cue" tone (85-dB, 2kHz) was played for 1 minute.

Open Field—At the beginning of each trial, the subject was placed in the center of the open-field apparatus and the subject's behavior was videotaped for the duration of the trial. The total number of line crossings for each trial was recorded over a 5-minute testing period.

Statistics

Statistics were performed using Prism 5.0 (GraphPad Software). Individual statistical tests performed are identified in Figure Legends. A *p*-value < 0.05 was considered significant and Bonferroni or Tukey *post hoc* tests were performed where appropriate to correct for multiple hypothesis testing. Tests for normality were performed where necessary using D'Agostino-Pearson omnibus test.

Supplementary Material

Refer to Web version on PubMed Central for supplementary material.

Acknowledgments

References

1. Amir RE, et al. Rett syndrome is caused by mutations in X-linked MECP2, encoding methyl-CpG-binding protein 2. Nat Genet. 1999; 23:185–188. [PubMed: 10508514]

2. Bienvenu T, Chelly J. Molecular genetics of Rett syndrome: when DNA methylation goes unrecognized. Nat Rev Genet. 2006; 7:415–426. [PubMed: 16708070]

3. Chahrour M, Zoghbi HY. The story of Rett syndrome: from clinic to neurobiology. Neuron. 2007; 56:422–437. [PubMed: 17988628]

4. Chen RZ, Akbarian S, Tudor M, Jaenisch R. Deficiency of methyl-CpG binding protein-2 in CNS neurons results in a Rett-like phenotype in mice. Nat Genet. 2001; 27:327–331. [PubMed: 11242118]

5. Guy J, Hendrich B, Holmes M, Martin JE, Bird A. A mouse Mecp2-null mutation causes neurological symptoms that mimic Rett syndrome. Nat Genet. 2001; 27:322–326. [PubMed: 11242117]

6. Shahbazian M, et al. Mice with truncated MeCP2 recapitulate many Rett syndrome features and display hyperacetylation of histone H3. Neuron. 2002; 35:243–254. [PubMed: 12160743]

7. Collins AL, et al. Mild overexpression of MeCP2 causes a progressive neurological disorder in mice. Hum Mol Genet. 2004; 13:2679–2689. [PubMed: 15351775]

8. Pelka GJ. Mecp2 deficiency is associated with learning and cognitive deficits and altered gene activity in the hippocampal region of mice. Brain. 2006; 129:887–898. [PubMed: 16467389]

9. Kerr B, Alvarez-Saavedra M, Sáez MA, Saona A, Young JI. Defective body-weight regulation, motor control and abnormal social interactions in Mecp2 hypomorphic mice. Hum Mol Genet. 2008; 17:1707–1717. [PubMed: 18321865]

10. Samaco RC, et al. A partial loss of function allele of methyl-CpG-binding protein 2 predicts a human neurodevelopmental syndrome. Hum Mol Genet. 2008; 17:1718–1727. [PubMed: 18321864]

11. Jentarra GM, et al. Abnormalities of cell packing density and dendritic complexity in the MeCP2 A140V mouse model of Rett syndrome/X-linked mental retardation. BMC Neurosci. 2010; 11:19. [PubMed: 20163734]

12. Guy J, Gan J, Selfridge J, Cobb S, Bird A. Reversal of neurological defects in a mouse model of Rett syndrome. Science. 2007; 315:1143–1147. [PubMed: 17289941]

13. Lioy DT, et al. A role for glia in the progression of Rett's syndrome. Nature. 2011 10.1038/nature10214

14. Ho KL, et al. MeCP2 binding to DNA depends upon hydration at methyl-CpG. Mol Cell. 2008; 29:525–531. [PubMed: 18313390]

15. Dani VS, et al. Reduced cortical activity due to a shift in the balance between excitation and inhibition in a mouse model of Rett syndrome. Proc Natl Acad Sci USA. 2005; 102:12560–12565. [PubMed: 16116096]

16. Dani VS, Nelson SB. Intact long-term potentiation but reduced connectivity between neocortical layer 5 pyramidal neurons in a mouse model of Rett syndrome. J Neurosci. 2009; 29:11263–11270. [PubMed: 19741133]

17. Wood L, Gray NW, Zhou Z, Greenberg ME, Shepherd GMG. Synaptic circuit abnormalities of motor-frontal layer 2/3 pyramidal neurons in an RNA interference model of methyl-CpG-binding protein 2 deficiency. J Neurosci. 2009; 29:12440–12448. [PubMed: 19812320]

18. Uhlhaas PJ, Singer W. Abnormal neural oscillations and synchrony in schizophrenia. Nat Rev Neurosci. 2010; 11:100–113. [PubMed: 20087360]

19. Gandal MJ, Edgar JC, Klook K, Siegel SJ. Gamma synchrony: Towards a translational biomarker for the treatment-resistant symptoms of schizophrenia. Neuropharmacology. 2011 10.1016/j.neuropharm.2011.02.007

20. Roberts TPL, et al. MEG detection of delayed auditory evoked responses in autism spectrum disorders: towards an imaging biomarker for autism. Autism Res. 2010; 3:8–18. [PubMed: 20063319]

21. Gandal MJ, et al. Validating γ oscillations and delayed auditory responses as translational biomarkers of autism. Biol Psychiatry. 2010; 68:1100–1106. [PubMed: 21130222]

22. Chao HT, et al. Dysfunction in GABA signalling mediates autism-like stereotypies and Rett syndrome phenotypes. Nature. 2010; 468:263–269. [PubMed: 21068835]

23. D'Cruz JA, et al. Alterations of cortical and hippocampal EEG activity in MeCP2-deficient mice. Neurobiol Dis. 2010; 38:8–16. [PubMed: 20045053]

24. Bader GG, Witt-Engerström I, Hagberg B. Neurophysiological findings in the Rett syndrome, II: Visual and auditory brainstem, middle and late evoked responses. Brain Dev. 1989; 11:110–114. [PubMed: 2712233]

25. Stauder JEA, Smeets EEJ, van Mil SGM, Curfs LGM. The development of visual- and auditory processing in Rett syndrome: an ERP study. Brain Dev. 2006; 28:487–494. [PubMed: 16647236]

26. Vacca M, et al. MECP2 gene mutation analysis in the British and Italian Rett Syndrome patients: hot spot map of the most recurrent mutations and bioinformatic analysis of a new MECP2 conserved region. Brain Dev. 2001; 23 (Suppl 1):S246–50. [PubMed: 11738884]

27. Schanen C, et al. Phenotypic manifestations of MECP2 mutations in classical and atypical Rett syndrome. Am J Med Genet A. 2004; 126A:129–140. [PubMed: 15057977]

28. Armstrong DD. Neuropathology of Rett syndrome. J Child Neurol. 2005; 20:747–753. [PubMed: 16225830]

29. Feng G, et al. Imaging neuronal subsets in transgenic mice expressing multiple spectral variants of GFP. Neuron. 2000; 28:41–51. [PubMed: 11086982]

30. Shahbazian MD, Antalffy B, Armstrong DL, Zoghbi HY. Insight into Rett syndrome: MeCP2 levels display tissue- and cell-specific differences and correlate with neuronal maturation. Hum Mol Genet. 2002; 11:115–124. [PubMed: 11809720]

31. Skene PJ, et al. Neuronal MeCP2 Is Expressed at Near Histone-Octamer Levels and Globally Alters the Chromatin State. Mol Cell. 2010; 37:457–468. [PubMed: 20188665]

32. Chahrour M, et al. MeCP2, a key contributor to neurological disease, activates and represses transcription. Science. 2008; 320:1224–1229. [PubMed: 18511691]

33. Nan X, Tate P, Li E, Bird A. DNA methylation specifies chromosomal localization of MeCP2. Mol Cell Biol. 1996; 16:414–421. [PubMed: 8524323]

34. Nuber UA, et al. Up-regulation of glucocorticoid-regulated genes in a mouse model of Rett syndrome. Hum Mol Genet. 2005; 14:2247–2256. [PubMed: 16002417]

35. Jones PL, et al. Methylated DNA and MeCP2 recruit histone deacetylase to repress transcription. Nat Genet. 1998; 19:187–191. [PubMed: 9620779]

36. Nan X, et al. Transcriptional repression by the methyl-CpG-binding protein MeCP2 involves a histone deacetylase complex. Nature. 1998; 393:386–389. [PubMed: 9620804]

37. Uhlhaas PJ, Pipa G, Neuenschwander S, Wibral M, Singer W. A new look at gamma? High- (>60 Hz) γ-band activity in cortical networks: function, mechanisms and impairment. Prog Biophys Mol Biol. 2011; 105:14–28. [PubMed: 21034768]

38. Tallon-Baudry C, Bertrand O. Oscillatory gamma activity in humans and its role in object representation. Trends Cogn Sci (Regul Ed). 1999; 3:151–162. [PubMed: 10322469]

39. Buzsáki G, Draguhn A. Neuronal oscillations in cortical networks. Science. 2004; 304:1926–1929. [PubMed: 15218136]

40. Winterer G, et al. Schizophrenia: reduced signal-to-noise ratio and impaired phase-locking during information processing. Clin Neurophysiol. 2000; 111:837–849. [PubMed: 10802455]

41. Foster BA, Coffey HA, Morin MJ, Rastinejad F. Pharmacological rescue of mutant p53 conformation and function. Science. 1999; 286:2507–2510. [PubMed: 10617466]

42. Kishi N, Macklis JD. MECP2 is progressively expressed in post-migratory neurons and is involved in neuronal maturation rather than cell fate decisions. Mol Cell Neurosci. 2004; 27:306–321. [PubMed: 15519245]

43. Uhlhaas PJ, Singer W. Neural synchrony in brain disorders: relevance for cognitive dysfunctions and pathophysiology. Neuron. 2006; 52:155–168. [PubMed: 17015233]

44. Ben-Ari Y. Developing networks play a similar melody. Trends Neurosci. 2001; 24:353–360. [PubMed: 11356508]

45. Goffin D, et al. Dopamine-dependent tuning of striatal inhibitory synaptogenesis. J Neurosci. 2010; 30:2935–2950. [PubMed: 20181591]

46. Zhou Z, et al. Brain-specific phosphorylation of MeCP2 regulates activity-dependent Bdnf transcription, dendritic growth, and spine maturation. Neuron. 2006; 52:255–269. [PubMed: 17046689]

47. Liao WL, et al. Modular patterning of structure and function of the striatum by retinoid receptor signaling. Proc Natl Acad Sci USA. 2008; 105:6765–6770. [PubMed: 18443282]

48. Canolty RT, et al. High gamma power is phase-locked to theta oscillations in human neocortex. Science. 2006; 313:1626–1628. [PubMed: 16973878]

49. Hardisty-Hughes RE, Parker A, Brown SDM. A hearing and vestibular phenotyping pipeline to identify mouse mutants with hearing impairment. Nat Protoc. 2010; 5:177–190. [PubMed: 20057387]
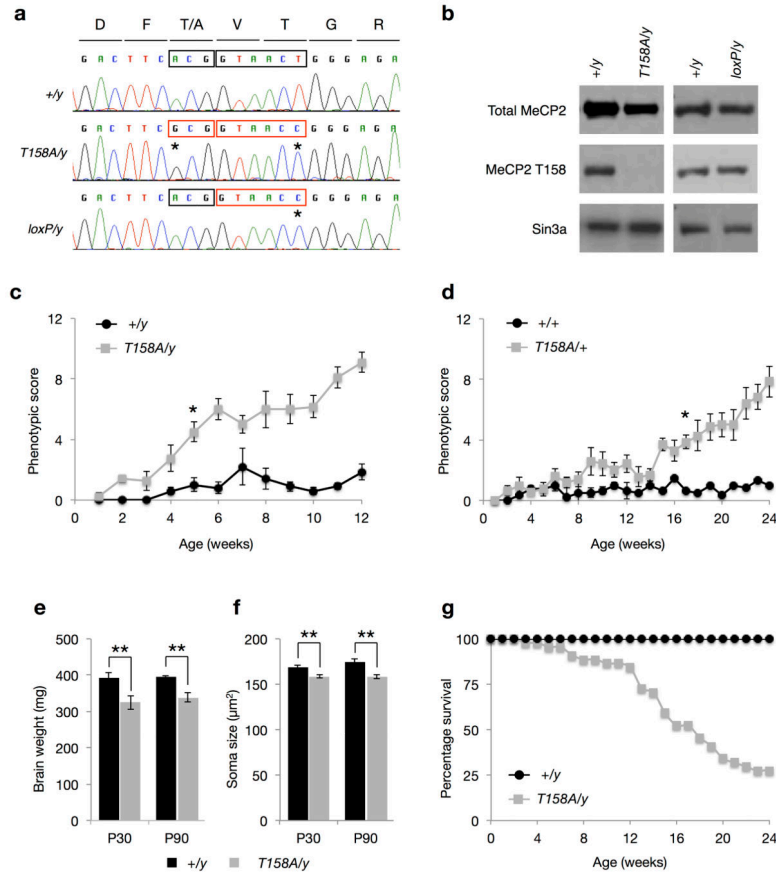
Figure 1. Generation and phenotypic characterization of MeCP2 T158A knockin mice
(a) Sequencing chromatogram of RT-PCR products from MeCP2 mRNA. Mutation of T158 codon ACG to Alanine codon GCG (first box) and creation of BstEII restriction site (second box) with a silent mutation are marked with a *. **(b)** Western blots probed with a site-specific MeCP2 T158 antibody, a total MeCP2 antibody and Sin3a antibody. **(c)** Developmental presentation of RTT-like phenotypes in male $Mecp2^{T158A/y}$ mice (n = 6; $F_{1,252}$ = 27.75, p-value < 0.0001; two-way ANOVA) relative to WT littermates (n = 5). Symbols represent mean score ± SEM. Phenotypic score is significantly higher in $Mecp2^{T158A/y}$ mice compared to WT littermates at 5 weeks and thereafter; * p-value < 0.05; two-way ANOVA with Bonferroni correction. **(d)** Developmental presentation of RTT-like phenotypes in female $Mecp2^{T158A/+}$ mice (n = 7; $F_{1,224}$ = 198.6, p-value < 0.0001; two-way ANOVA) relative to $Mecp2^{+/+}$ littermates (n = 6). Phenotypic score is significantly higher in $Mecp2^{T158A/+}$ mice compared to WT littermates at 17 weeks and thereafter; * p-value < 0.05; two-way ANOVA with Bonferroni correction. **(e)** Brain weights at P30 (n = 4 for both genotypes) and P90 (n = 6 for both genotypes). Bars represent mean ± SEM. ** p-value < 0.01; two-tailed t-test with Bonferroni correction. **(f)** Soma size in hippocampal CA1 pyramidal neurons. Bars represent mean ± SEM (n = 100 cells from 5 animals per genotype). ** p-value < 0.01; two-tailed t-test with Bonferroni correction. **(g)** Survival of male $Mecp2^{T158A/y}$ (n = 43) and $Mecp2^{+/y}$ littermates (n = 43).
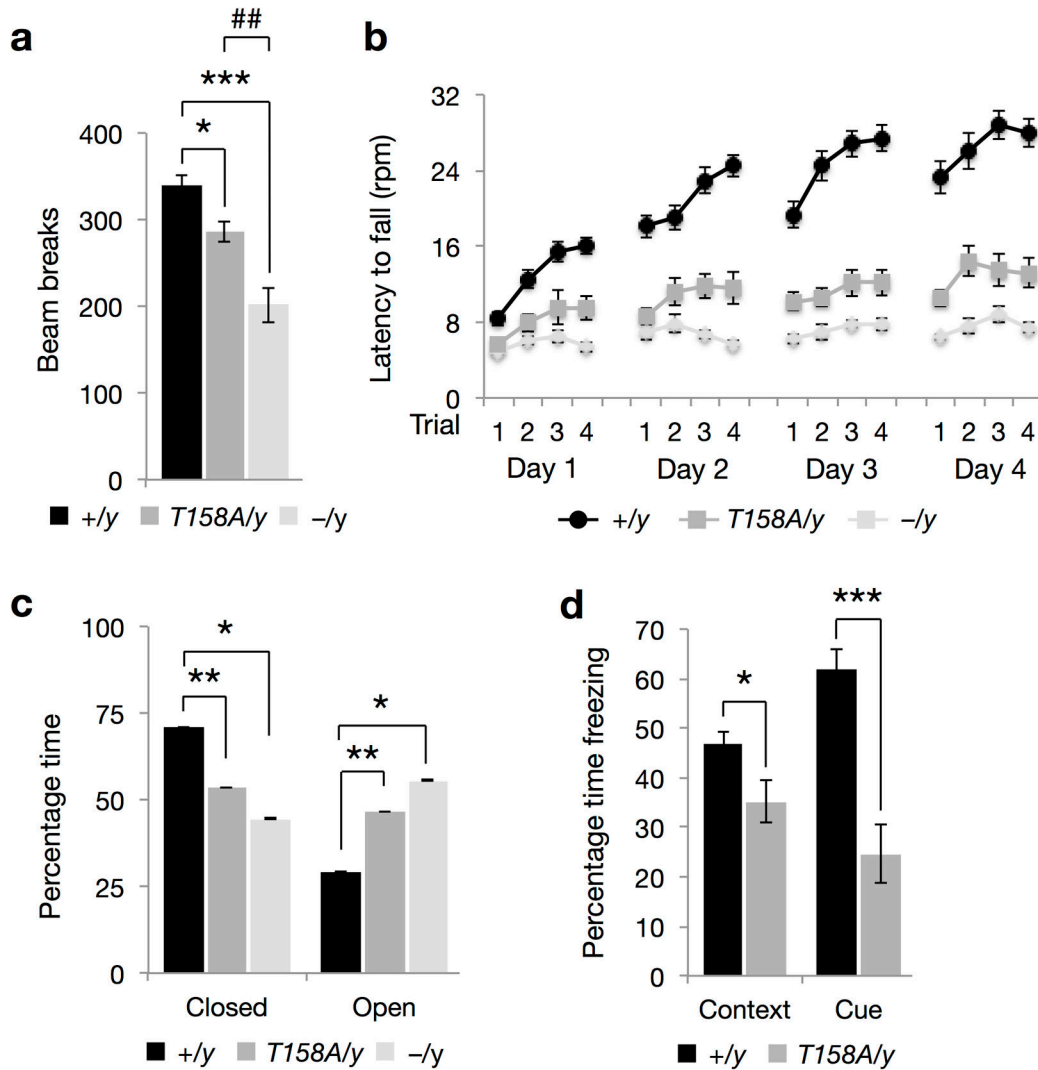
Figure 2. Behavioral characterization of MeCP2 T158A mice
(a) Locomotor activity in $Mecp2^{T158A/y}$ mice (n = 15), $Mecp2^{-/y}$ mice (n = 14) and $Mecp2^{+/y}$ littermates (WT; n = 33) at 9 weeks of age. Bars represent mean ± SEM. * p-value < 0.01, *** < 0.001 and ## < 0.01; one-way ANOVA with Tukey's *post hoc* test. (b) Motor coordination and motor learning assessed using a rotarod assay in $Mecp2^{T158A/y}$ mice (n = 16; $F_{1,645}$ = 447.2, p-value < 0.0001; two-way ANOVA) and $Mecp2^{-/mice}$ (n = 14; $F_{1,602}$ = 841.46, p-value < 0.0001; two-way ANOVA) and WT littermates (n = 27) at 9 weeks of age. The deficit in $Mecp2^{-/y}$ mice is significantly more than that observed in $Mecp2^{T158A/y}$ mice ($F_{1,437}$ = 83.82, p-value < 0.0001; two-way ANOVA). Symbols represent mean ± SEM. (c) Anxiety-like behavior in $Mecp2^{T158A/y}$ mice (n = 15) and $Mecp2^{-/y}$ mice (n = 11) measured using elevated zero maze compared to WT littermates (n = 32) at 9 weeks of age. Bars represent mean ± SEM. * p-value < 0.05 and ** < 0.01; one-way ANOVA with Tukey's *post hoc* test. (d) Learning and memory assessed using context-and cue-dependent fear conditioning in $Mecp2^{T158A/y}$ mice (n = 16) and WT littermates (n = 33) at 10 weeks of age.

Bars represent mean ± SEM. * p-value < 0.05 and *** < 0.001; two-tailed t-test with Bonferroni correction.
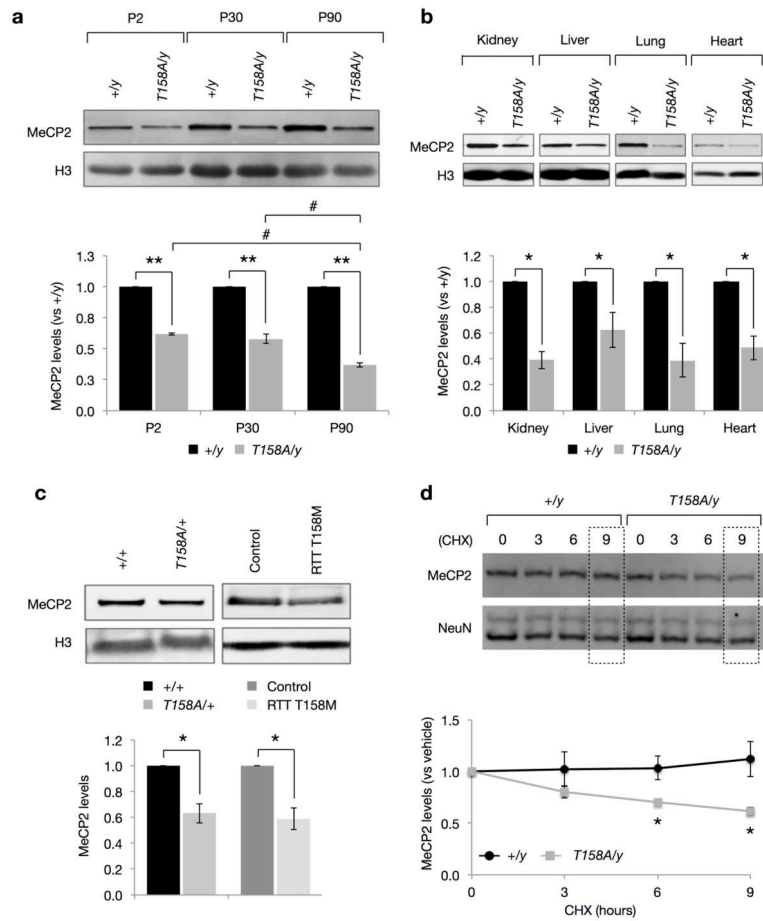
Figure 3. Decreased MeCP2 protein stability in MeCP2 T158A mice
(a) MeCP2 protein levels in forebrains of *Mecp2*[T158A/y] mice at P2, P30, and P90 compared to *Mecp2*[+/y] littermates (n = 3 for each genotype). Bars represent mean ± SEM. ** *p*-value < 0.01; one-sample t-test with Bonferroni correction. # < 0.05; one-way ANOVA with Tukey's *post hoc* test. **(b)** MeCP2 protein levels are significantly reduced in kidney, liver, lung and heart tissues of *Mecp2*[T158A/y] (n = 3) compared to *Mecp2*[+/y] littermates at P90 (n = 3). Bars represent mean ± SEM. * *p*-value < 0.05; one-sample t-test with Bonferroni correction. **(c)** MeCP2 protein levels in female *Mecp2*[T158A/+] mice (n = 3) and *Mecp2*[+/y] littermates at P90 (n = 3). MeCP2 protein levels in fibroblasts derived from a female RTT patient carrying the MeCP2 T158M mutation compared to fibroblasts derived from an age-matched female control (n = 3 separate passages). Bars represent mean ± SEM. * *p*-value < 0.05; one-sample t-test. **(d)** E16 + 7 DIV cortical neurons derived from *Mecp2*[T158A/y] (n = 3) and *Mecp2*[+/y] littermates (n = 3) were treated with vehicle (0) or 100 μM Cycloheximide (CHX) for 3, 6 or 9 hours. Bars represent mean MeCP2 levels relative to vehicle ± SEM. * *p*-value < 0.05; two-way ANOVA with Bonferroni correction.
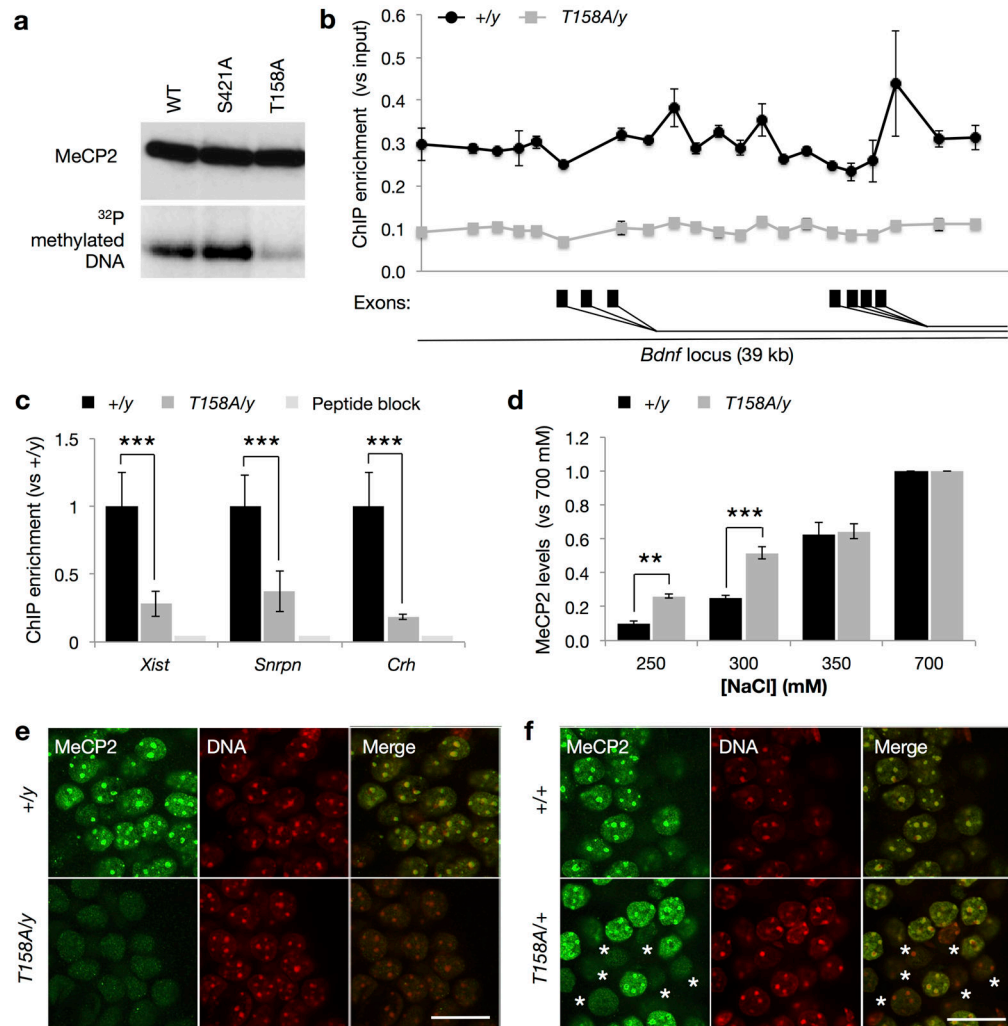
Figure 4. Reduced MeCP2 binding to methylated DNA in T158A mice

(a) MeCP2 binding to methylated DNA (methylated oligonucleotides spanning the −148 CpG site of Bdnf promoter IV) is reduced by T158A mutation relative to WT and MeCP2 S421A mutation in Southwestern assay. **(b)** MeCP2 binding across a 39 kb of the promoter region of the *Bdnf* locus in brains obtained from *Mecp2^T158A/y* mice mice and *Mecp2^{+/y}* littermates (n = 3; two-way ANOVA, $F_{1,84} = 639.1$, *p*-value < 0.0001). Symbols represent mean ± SEM. Alternative *Bdnf* exons are indicated with black rectangles. **(c)** MeCP2 binding to the *Xist*, *Snrpn*, and *Crh* loci in *Mecp2^T158A/y* mice (n = 3) compared to *Mecp2^{+/y}* littermates (n = 3). Bars represent mean ± SEM. *** *p*-value < 0.001; two-tailed t-test with Bonferroni correction. **(d)** Salt extraction of WT MeCP2 and MeCP2 T158A protein with increasing concentrations of NaCl (n = 3). Bars represent mean ± SEM normalized to MeCP2 levels extracted with 700 mM NaCl. ** *p*-value < 0.01 and *** < 0.001; two-way ANOVA with Bonferroni correction. **(e)** MeCP2 co-localization with heterochromatin-dense foci in male WT but not *Mecp2^T158A/y* mice at P90. Representative images of neuronal nuclei shown are single confocal planes at 100X magnification. Scale bar corresponds to 20

μm. **(f)** MeCP2 staining in nuclei obtained from female *Mecp2^{T158A/+}* mice. Nuclei showing diffuse MeCP2 staining are marked with an *. Scale bar corresponds to 20 μm.
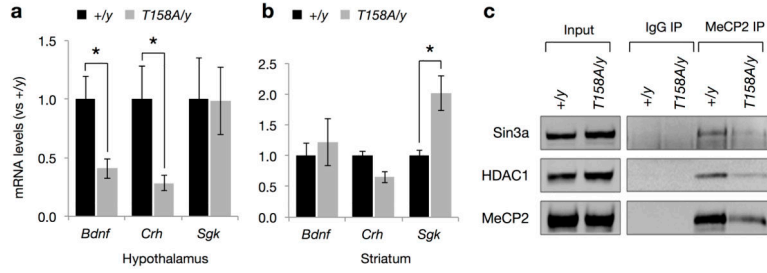
Figure 5. Disruption of MeCP2 methyl-DNA binding leads to deregulation of gene expression
(a) *Bdnf*, *Crh* and Sgk mRNA expression in the hypothalamus of *Mecp2*$^{T158A/y}$ mice compared to *Mecp2*$^{+/y}$ littermates (n = 4). Bars represent mean ± SEM. * *p*-value < 0.05; two-tailed t-test with Bonferroni correction. **(b)** *Bdnf*, *Crh* and Sgk mRNA expression in the striatum of *Mecp2*$^{T158A/y}$ mice and *Mecp2*$^{+/y}$ littermates (n = 4). Bars represent mean ± SEM. * *p*-value < 0.05; two-tailed t-test with Bonferroni correction. **(c)** MeCP2 T158A mutation does not impair the association of MeCP2 with HDAC1 or Sin3a. MeCP2 immunoprecipitation from brain nuclear extracts prepared from *Mecp2*$^{T158A/y}$ and *Mecp2*$^{+/y}$ littermates are probed with indicated antibodies.
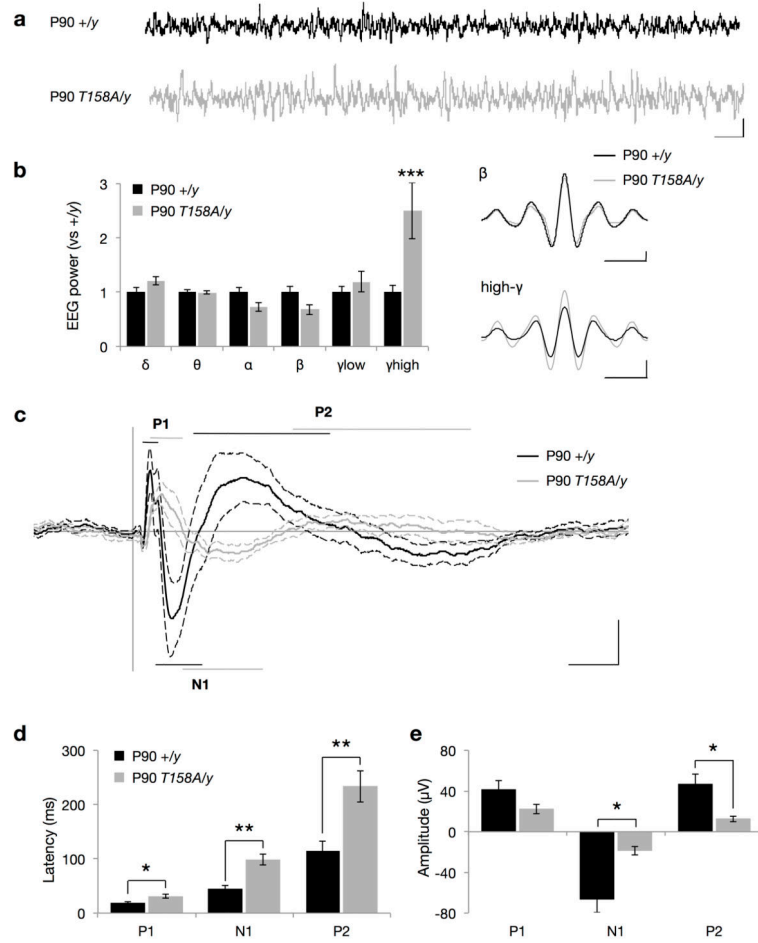
Figure 6. EEG and ERP recordings in MeCP2 T158A mice
(a) Representative EEG traces from awake, freely mobile mice. Scale bar corresponds to 1 second (horizontal) and 200 μA (vertical). **(b)** Basal EEG power measurements in P90 $Mecp2^{T158A/y}$ mice (n = 7) compared to $Mecp2^{+/y}$ littermates (n = 8). Frequency bands are represented as follows: δ (2–4 Hz), θ (4–8 Hz), α (8–12 Hz), β (12–30 Hz), low-γ (30–50 Hz), and high-γ (70–140 Hz). Insets show β and high-γ mean amplitudes across EEG recordings. Scale bars represent one oscillation cycle (horizontal) and 20 μA (vertical). Bars represent mean ± SEM. *** p-value <0.001; two-tailed t-test with Bonferroni correction. **(c)** Grand average event-related potential (ERP) traces following presentation of 85-dB white-noise clicks with 4-second interstimulus intervals. Traces represent mean amplitude (solid line) ± SEM (dashed lines). The characteristic polarity peaks P1, N1 and P2 are highlighted with straight lines with the length indicating latency range. Scale bar corresponds to 50 ms (horizontal) and 20 μA (on vertical). **(d)** Latencies and **(e)** amplitudes of ERP peaks. Bars represent mean ± SEM. * p-value < 0.05 and ** < 0.01; two-tailed t-test with Bonferroni correction
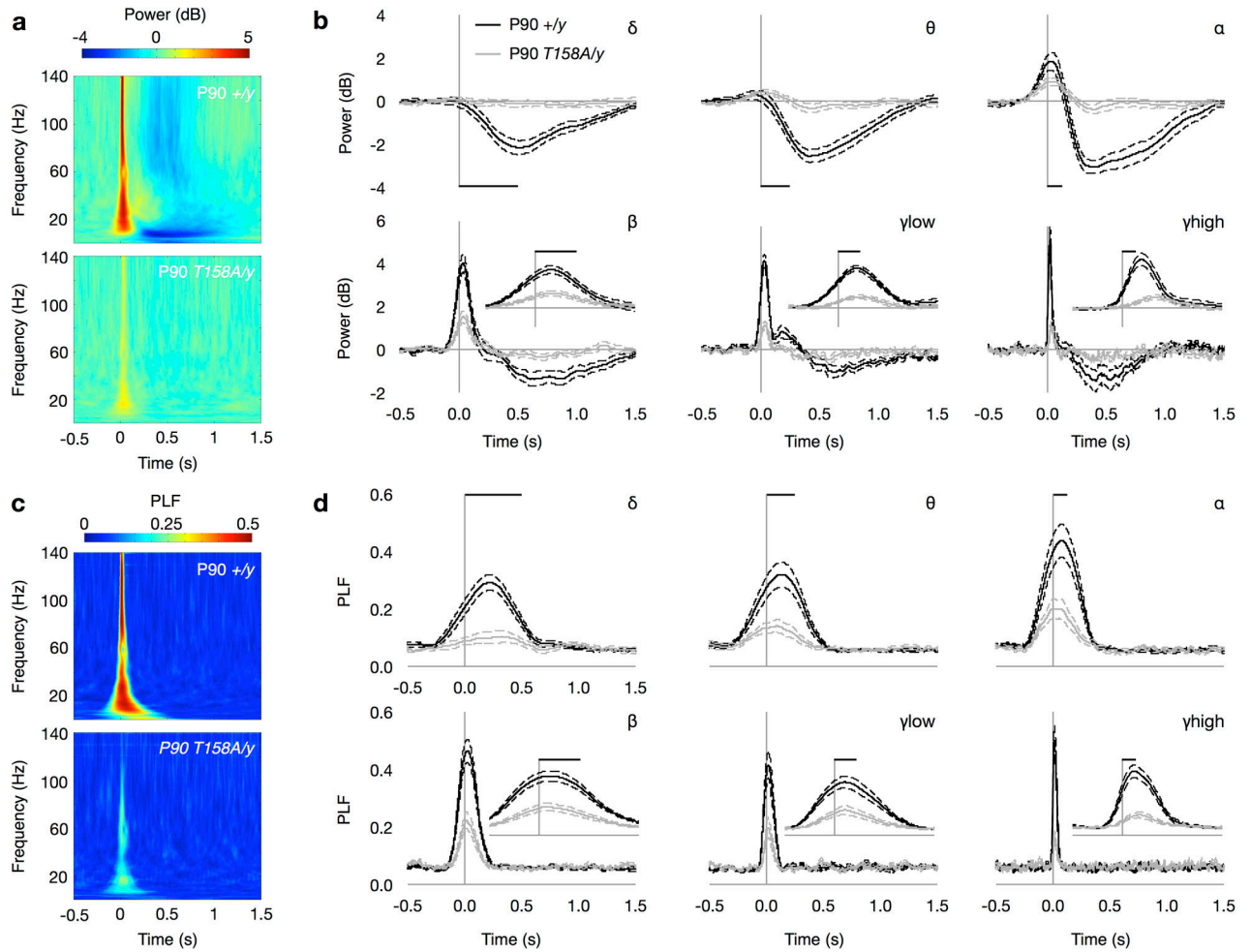
Figure 7. Decreased event-related power and PLF in *Mecp2^T158A/y* mice
(a) Time-frequency plots showing changes in event-related power in response to 85-dB auditory stimulation in P90 *Mecp2^T158A/y* mice and *Mecp2^+/y* littermates. Time is plotted on the abscissa (where *t = 0* at sound presentation) and frequency on the ordinate. Color represents mean power with warmer colors corresponding to an increased power and cooler colors representing decreased power compared to pre-stimulus baseline. **(b)** Changes in event-related mean power averaged across δ (2–4 Hz), θ (4–8 Hz), α (8–12 Hz), β (12–30 Hz), low-γ (30–50 Hz), and high-γ (70–140 Hz) frequencies. Scale bars represent the length of a single oscillation cycle of the lowest frequency in the range. Insets showed power traces on expanded time-scale denoted by length of single oscillation cycle. Traces represent mean power ± SEM. **(c)** Time-frequency plots showing changes in event-related phase locking factor (PLF) in response to 85-dB auditory stimulation. Color represents PLF with warmer colors corresponding to a higher PLF or lower circular variance in EEG phase across trials. **(d)** Changes in event-related PLF averaged across frequencies as above. Scale bars represent the length of a single oscillation cycle and insets show traces on expanded time-scale. Traces represent mean PLF ± SEM.
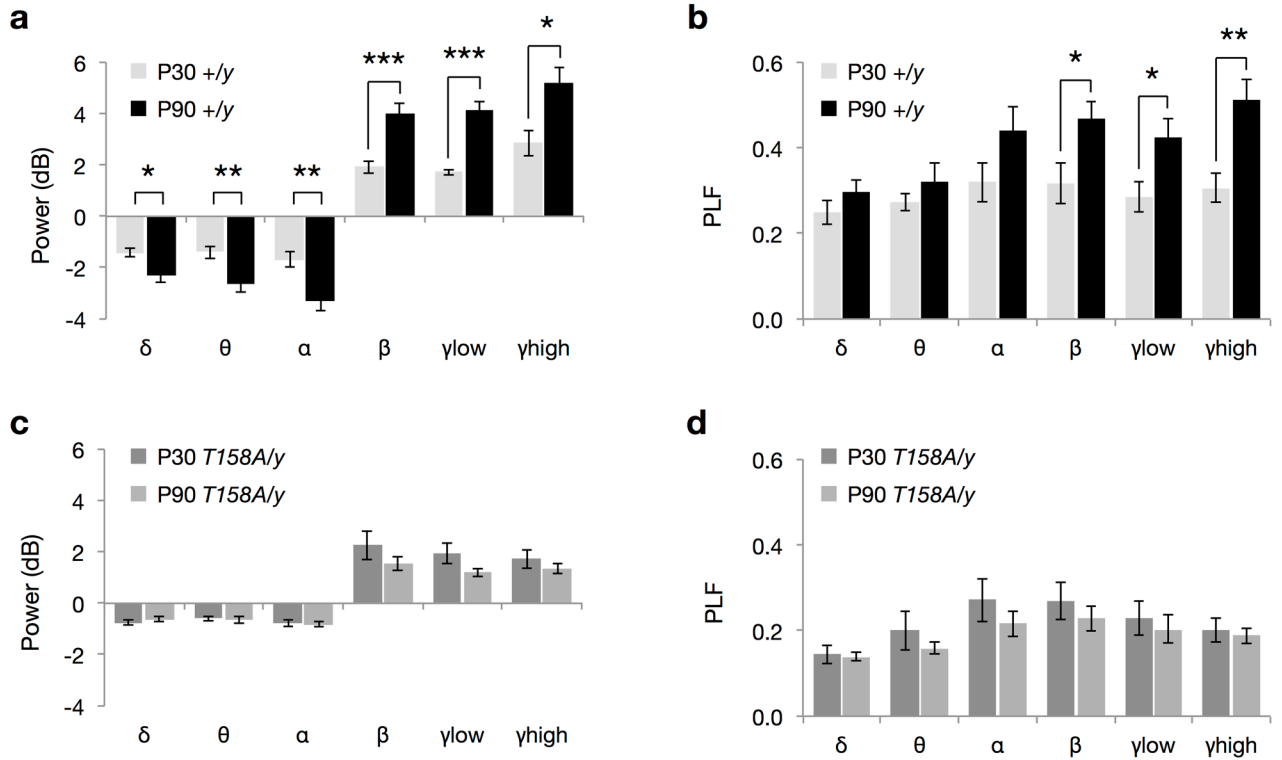
**Figure 8. Age-dependent increase in event-related power and PLF is absent in *Mecp2^{T158A/y}*
mice**

(a) Event-related power changes in *Mecp2^{+/y}* (WT) mice at P30 and P90. (b) Event-related
phase-locking factor (PLF) changes in WT mice at P30 and P90. (c) Event-related power
changes in *Mecp2^{T158A/y}* mice at P30 and P90. (d) Event-related PLF changes in
Mecp2^{T158A/y} mice at P30 and P90. Bars represent mean ± SEM. * p-value < 0.05, ** < 0.01
and *** < 0.001; two-tailed t-test with Bonferroni correction.